Accepted Manuscript

Improving GLONASS Orbit Quality by Re-estimating Satellite Antenna Offsets

Rolf Dach, Andreja Sušnik, Andrea Grahsl, Arturo Villiger, Stefan Schaer, Daniel Arnold, Lars Prange, Adrian Jäggi

Please cite this article as: Dach, R., Sušnik, A., Grahsl, A., Villiger, A., Schaer, S., Arnold, D., Prange, L., Jäggi, A., Improving GLONASS Orbit Quality by Re-estimating Satellite Antenna Offsets, *Advances in Space Research* (2019), doi: https://doi.org/10.1016/j.asr.2019.02.031

Improving GLONASS Orbit Quality
by Re-estimating Satellite Antenna Offsets

Rolf Dach[a][*], Andreja Sušnik[a,b], Andrea Grahsl[a], Arturo Villiger[a], Stefan Schaer[c], Daniel Arnold[a], Lars Prange[a], and Adrian Jäggi[a][*]

[a] *Astronomical Institute, University of Bern, Sidlerstrasse 5, CH-3012 Bern, Switzerland*
[b] *now with School of Civil Engineering and Geosciences, Newcastle University, Newcastle, NE1 7RU, UK*
[c] *Swiss Federal Office of Topography, swisstopo, Seftigenstrasse 264, CH-3084 Wabern, Switzerland*

Abstract

Earlier studies performed at the Center for Orbit Determination in Europe (CODE) analysis center have revealed conspicuous signatures for certain GLONASS satellites when comparing their orbits with Satellite Laser Ranging (SLR) measurements. In this study we show that this phenomenon can be significantly reduced when using horizontal satellite antenna offsets that differ from the nominal values used by the International GNSS Service (IGS) for specific intervals and satellites.

Analysis of multi-year time series shows instantaneous changes in the satellite antenna offset parameters of several centimeters in the X- and Y-component whereas the Z-component is not affected. In some cases the offsets do not agree with the nominal values during the entire lifetime of the satellite. The magnitude of the deviation may vary between 5 to 15 cm. Using these re-estimated satellite antenna offsets in the orbit determination the residuals with respect to the Satellite Laser Ranging (SLR) measurements are significantly reduced whereas the orbit misclosures for one-day arcs are too noisy to detect a positive or negative impact.

It is difficult to reconstruct from the available information what actually caused the observed changes. However, changes in the carrier-to-noise density reported in the observation files in Receiver INdependent EXchange format (RINEX) by several IGS stations suggest an issue with the satellite antennas.

Keywords: GLONASS orbit determination, SLR residuals for GLONASS, Satellite antenna offsets

1. Background and Motivation

The International GNSS Service (IGS, Johnston et al, 2017, where GNSS stands for Global Navigation Satellite System) is preparing itself for the full inclusion of the currently new constellations, like the European Galileo, Chinese BeiDou, Japanese QZSS (Quasi-Zenith Satellite System), and Indian NAVIC (Navigation Indian Constellation) into the operational processing in the frame of the IGS multi-GNSS extension (MGEX, Montenbruck et al, 2017). The International GLONASS Experiment (IGEX, Willis et al, 2000) has taken a similar effort in the 90ies of the last century in order to prepare for the inclusion of GLONASS – the Russian counterpart to GPS – into the IGS processing scheme. The effort lasted longer than initially expected because of the limited number of available GLONASS satellites for a long time. With the launches of GLONASS-M satellites with a much longer lifetime than the first generation of GLONASS satellites

during the noughties the number of available satellites continuously increased. Since the end of 2011, the GLONASS constellation is fully deployed with the nominal number of 24 satellites.

In May 2003 the Center for Orbit Determination in Europe (CODE) started with the rigorously combined analysis of the measurements from both GPS and GLONASS systems as the first analysis center of the IGS, see Dach et al (2009). Advantages of fully combined analysis of observations from both systems have also been demonstrated by Springer and Dach (2010) and later by other authors. Meanwhile other analysis centers follow this approach: currently five for the ultra-rapid and six for the final products of the IGS (Moore and Herring, 2018). In this way, GLONASS is established as the second complete GNSS constellation not only within the IGS but also on the user side, where the combined processing of GPS and GLONASS measurements has become standard (e.g., nearly all analysis centers within EUREF Permanent Network (EPN) include GLONASS in their product analysis, see Bruyninx et al, 2018). Such groups expect similar high quality IGS orbit products for GLONASS as it is the case for GPS.

---
[*]Corresponding author at Astronomical Institute, University of Bern, Sidlerstrasse 5, CH-3012 Bern, Switzerland
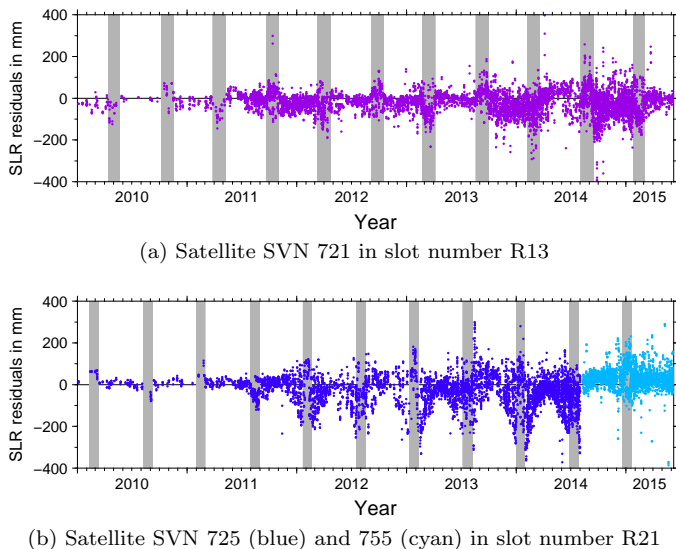
Email address: rolf.dach@aiub.unibe.ch (Rolf Dach[a])

(a) Satellite SVN 721 in slot number R13

(b) Satellite SVN 725 (blue) and 755 (cyan) in slot number R21

Figure 1: SLR residuals of satellites as obtained in Grahsl et al (2016) in selected slot numbers. Gray bars denote eclipse seasons.

While developing the extension of the Empirical CODE Orbit Model (ECOM) at CODE it was noticed that two of the GLONASS satellites showed an unexpected behavior. As a consequence the two satellites were excluded from the orbit validation using Satellite Laser Ranging (SLR) measurements (see Sect. 6 in Arnold et al, 2015). In a follow-up study conducted by Prange et al (2016), the list of GLONASS satellites with specifically higher SLR residuals had to be further extended.

At first glance one could suspect this to be a weakness of the new solar radiation pressure (SRP) modeling (named ECOM2). However, inspecting Fig. 1 this explanation seems to be unlikely. In Fig. 1a the magnitude of the discrepancy between the microwave-based orbits and the SLR measurements doubles after the second eclipse season of the year 2013. Other examples for instantaneous degradation of the SLR validation are shown for instance in Grahsl et al (2016). There is a set of GLONASS satellites where the differences to the SLR measurements show the expected behavior only for the first years of their lifetime. Starting from a certain epoch, they become instantaneously larger by a factor of two or even more.

In the same context, the example of exchanging the space vehicles in the slot R21 in August 2014 is interesting (already reported by Prange et al, 2016). The satellite with SVN 725 was launched in September 2008. The SLR tracking to this satellite is sparse in the first year but the validation shows the expected behavior until November 2011 when the values significantly increase (see Fig. 1b). In August 2014, this satellite was decommissioned and replaced by a new one (SVN 755, cyan dots in Fig. 1b) into the same slot. For the new space vehicle the magnitude of the differences to the SLR measurements becomes again much smaller.

In case of a deficiency in the ECOM2, the same behav-

ior for both space vehicles (both are of the same GLONASS-M type) would have been expected, because the geometry between the Sun, Earth, and the satellite directly before and after the satellite exchange is still comparable. Because the pattern in the SLR validation is changing with the exchange of the space vehicle, it is more likely that "something unexpected" happened at the satellite (which cannot be absorbed by the orbit model). Also in cases of an instantaneous increase of the SLR validation values (some examples are given above) the geometry between Sun, Earth, and the satellites does not significantly change before and after the degradation of the satellite orbits.

An SLR validation for the GLONASS orbit solutions from other IGS analysis centers (e.g., ESA or GFZ) also show a change in the pattern after SVN 725 has been replaced by SVN 755 in August 2014. This excludes potential mismodeling in the Bernese GNSS Software (Dach et al, 2015) used at CODE for the data analysis as an explanation.

In this paper we demonstrate how to significantly improve the orbit quality for these periods (Sect. 3) after a description of the data analysis in Sect. 2. The orbit improvement is confirmed in Sect. 4 where different orbit validation methods are applied. Finally, in Sect. 5 potential effects onboard the satellites are discussed that could explain the observed phenomena. The paper concludes with a summary in Sect. 6.

2. Data Analysis

Sušnik et al (2017) provide a reprocessing series of measurements from GNSS generated at Astronomical Institute of the University of Bern (AIUB) in the frame of the European Gravity Service for Improved Emergency Management (EGSIEM) project (Jäggi et al, 2015). The station selection and most of the processing characterization correspond to CODE's reprocessing effort (Steigenberger et al, 2014) for the IGS. Because the antenna phase center correction model IGS 08 (Schmid et al, 2016) was still used for the data processing, the solution is expected to be fully compatible to the ITRF2014 reference frame (Altamimi et al, 2016) which is based on the same antenna correction model. As a consequence, for about 90% of the stations in the network (see Fig. 2) station coordinates are known in the reference frame and can be used for the datum definition.

Regarding the tracking of GLONASS satellites, the map in Fig. 2 reflects a situation that is typical for the early years of the reprocessing, where most of the stations are located in Europe. The situation starts to improve in the year 2006. Since about 2010, a fully global coverage of GLONASS tracking stations is available.

The main difference with respect to the previous reprocessing series (Steigenberger et al, 2014) is the use of the ECOM2 according to Arnold et al (2015). In contrast to Sušnik et al (2017) only the twice-per-revolution periodic terms in D-direction (oriented from the satellite to

3

the Sun) have been estimated in addition to the classical ECOM parameters as proposed by Springer (1999). As in recent reprocessing series the attitude of the GPS and GLONASS satellites is handled according to Kouba (2009) and Dilssner et al (2011), respectively.

From the above mentioned reprocessing series the daily normal equations (NEQs) are used for further processing. They contain all necessary information such as station coordinates, station-wise troposphere zenith path delays (with 2 hours sampling, based on Vienna Mapping Function, VMF1, Böhm et al, 2006) and gradient parameters (daily sampling, based on Chen and Herring, 1997), Earth rotation parameters (polar motion and their rates, as well as length of day), dynamical satellite orbit parameters (apart from the initial conditions, seven SRP parameters of the ECOM2 according to Arnold et al, 2015), empirical velocity changes of the satellites every 12 hours (as described in Beutler et al, 1994), and satellite antenna offset (SAO) parameters.

The reprocessing ends in May 2015 (day of year 150). After that date the NEQs from the operational final solution series, produced by CODE for the IGS were used. Until end of January 2017 (before the switch to the new IGS 14 antenna model/reference frame in GPS week 1934, January 29, 2017, see IGSMAIL #7399) they are consistent with the reprocessing solution.

3. Satellite Antenna Corrections

3.1. Estimating satellite antenna offset corrections

In order to obtain stable orbits (also for the early years of the sparse GLONASS tracking network), three consecutive NEQs were combined to a three-day long-arc solution. The related theory was developed in Beutler et al (1996); benefits and disadvantages are, e.g., discussed in Lutz et al (2016). Seven of such three-day solutions were stacked to a weekly solution where the orbits and Earth rotation parameters (ERPs) are kept independently by pre-eliminating the related parameters before stacking com-

(a) GPS satellite: SVN 044; PRN G28

(b) GLONASS satellite: SVN 732; slot number R23

Figure 3: Time series of estimated horizontal satellite antenna offset (SAO) where the nominal values that are used for the IGS processing are indicated by the dashed gray lines that are typically below the thick horizontal line indicating the long-term solution. In addition the elevation angle of the Sun above the orbital plane (so-called beta angle) is given.

mon parameters. The weekly coordinates are compared with the coordinate set derived for the particular week from the ITRF2014 reference frame. If the agreement is better than 1 cm for the horizontal and 2.5 cm for the vertical components, the related station was included in a minimum constrained solution for the datum definition based on no-net-translation, no-net-rotation, and no-scale-change conditions.

Typically, one set of SAO corrections is estimated over the entire lifetime of each satellite. Afterwards, each weekly solution may be compared to the long-term solution in order to derive the repeatability for the SAO correction estimates as a quality measure. Examples for two satellites are provided in Fig. 3 where the long-term solution is shown as a thick horizontal line and the weekly solutions as dots together with their error bars. In particular for the GLONASS satellite in Fig. 3b large variations in the weekly solutions are visible that are reflected in significantly increased error bars. The variation of the formal errors and the pattern in the weekly solutions for the horizontal SAO-components is not limited to the GLONASS but also visible for the GPS satellites (see Fig. 3a). Since
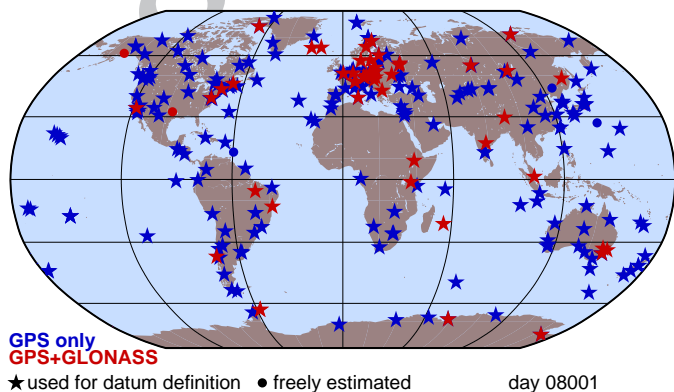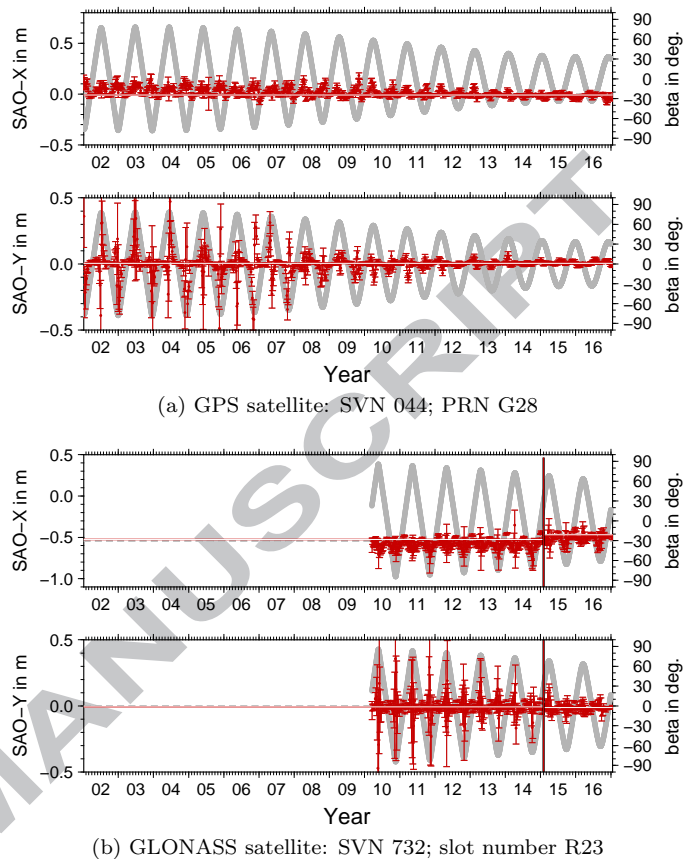

Figure 2: Geographical distribution of the stations (shown for January 1st, 2008) where the reference stations of the ITRF2014 solution are indicated.

the variations in the formal errors are more pronounced for the GLONASS satellites, it is here in particular necessary to derive the long-term solutions by taking into account the full covariance information.

The variability of the formal errors of the horizontal SAO parameters can be explained by the correlation with the SRP parameters (see, e.g., Schmid and Rothacher, 2003): if the Sun is perpendicular to the orbital plane (the angle beta referring to the elevation of the Sun above the orbital plane becomes $\pm 90°$), the direction of the SAO-X component coincides with the D-direction of the ECOM decomposition, whereas the SAO-Y component corresponds to the orbit parameter in the Y-direction in the ECOM decomposition (along the solar panel axis in order to absorb the effect from the Y-bias). If the Sun is located in the orbital plane (beta angle is close to zero), the satellite body-fixed coordinate system (where the SAO parameters are referring to) and the Sun-oriented coordinate system in the satellites (relevant for the SRP modeling) do not coincide, allowing for the discrimination of the parameters.

Fortunately, for none of the GNSS satellites the Sun is exactly perpendicular to the orbital plane. Due to the higher inclination of the GLONASS orbits the elevation of the Sun above the orbital plane may become $i + \epsilon = 65° + 23° = 88°$ (with i being the inclination of the orbital plane and ϵ the obliquity of the ecliptic with respect to Earth's equator), whereas the similar unfavorable scenario for GPS satellites is limited to $56° + 23° = 79°$. Only one of the orbital planes in the constellation may be affected by this maximum elevation of the Sun. Due to nodal precession, the maximum elevation of the Sun changes with time for each orbital plane. This can nicely be seen in Fig. 3a by the decreasing size of the affected error bars.

In contrast to Schmid et al (2007) also the eclipse periods have been used for the estimation of the SAO parameters. First, these are the periods with low formal errors for the SAO parameters and they are for that reason in particular valuable. Second, the orbit modeling has been significantly advanced with respect to the work of Schmid and Rothacher (2003), e.g., regarding the attitude handling for the GLONASS satellites and the extension of the orbit model – the additional terms in the ECOM2 model help in particular to improve the orbits if the Sun is close to the orbital plane (Arnold et al, 2015).

3.2. Detecting discontinuities

Figure 3b shows a jump in the estimated SAO-X parameters at the beginning of 2015 (indicated by the vertical line). Such discontinuities in the time series can be observed for a number of GLONASS satellites in the X- as well as in the Y-components. Interestingly, such events are typically not connected to a significant change in the Z-component of the estimated SAOs. After verifying this the further solutions presented in this paper are generated without estimation the SAO-Z parameters but forcing them to the values of the IGS 08 antenna model.

The detection of the discontinuities in the SAO time series is not straightforward because of the varying uncertainties. As mentioned above the detection algorithm needs to consider the full covariance information. For that reason, a series of annual solutions was computed by combining 50 subsequent weekly NEQs: $\mathrm{SAO}_{annual(n)} = \mathrm{SAO}_{week(n)} + \cdots + \mathrm{SAO}_{week(n+50)}$. This type of annual solution is shifted from week to week in order to obtain a kind of running mean annual SAO solutions:

$$
\begin{aligned}
\mathrm{SAO}_{annual(n)} &= \mathrm{SAO}_{week(n)} + \cdots + \mathrm{SAO}_{week(n+50)} \\
\mathrm{SAO}_{annual(n+1)} &= \mathrm{SAO}_{week(n+1)} + \cdots + \mathrm{SAO}_{week(n+51)} \\
\mathrm{SAO}_{annual(n+2)} &= \mathrm{SAO}_{week(n+2)} + \cdots + \mathrm{SAO}_{week(n+52)} \\
&\vdots
\end{aligned}
$$

This operation is illustrated as step 1 in Fig. ??. The lightblue bars are related to the series of annual solutions obtained by shifting the original weekly solutions week-by-week whereas the blue bar just indicates one example such an annual solution (e.g., $\mathrm{SAO}_{annual(n)}$). All annual solutions containing a discontinuity will be affected by it depending on whether the discontinuity is located at the beginning, in the middle or towards the end of the interval as indicated in the scheme in Fig. ??.

This allows to detect the discontinuity also in the series of annual solutions, indicated as step 2 in Fig ??. The difference between the annual SAO estimates from the solution $\mathrm{SAO}_{annual(n)}$ (covering the weeks $n \ldots n + 50$) and $\mathrm{SAO}_{annual(n+50)}$ (including the weeks $n + 50 \ldots n + 100$) is used for the detection of the discontinuities. The differences between the two annual solutions indicated by the two red bars are computed. The series of differences is displayed as red dots in Fig. ??.

These series of differences have a local maximum/minimum if solution $\mathrm{SAO}_{annual(n)}$ ends before a discontinuity epoch and solution $\mathrm{SAO}_{annual(n+50)}$ starts after this epoch. The discontinuity is assumed for epoch $n + 50$. In Fig. ?? the detected epoch is indicated by the gray circle behind the red dot. It corresponds to the epoch of discontinuity in the original SAO time series.

The use of 50 instead of 52 weeks for the annual solutions is related to the fact that it covers 350 instead of 365 days. The pattern in the formal errors discussed in Sect. 3.1 are related to the location of the Sun with respect to the orbital plane which repeats with a 354 days period for the GLONASS constellation (draconitic period).

Two additional conditions were considered: first, the local maximum/minimum needs to have a magnitude of at least 3 cm in order to distinguish between events and noise. The threshold has been established by empirical experiments. The second condition is that an annual SAO solution needs to be based on at least 300 days for a particular satellite to be considered as sufficiently reliable for the algorithm. Because the series of consistent NEQs ends in January 2017, only events until March 2016 can be detected with this approach.

5
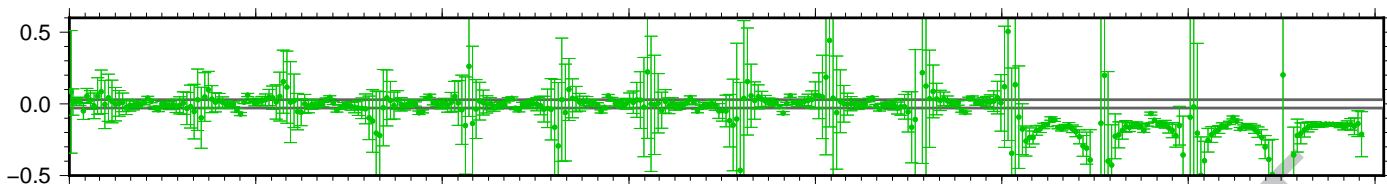
3.3. Summary of the SAO results

With the above described algorithm in total 40 events could be detected in the processed time series. Some of the satellites showed two or even more changes of the estimated horizontal SAO corrections. There are also satellites where the estimated long-term SAO values deviate more than 3 cm from the beginning of the satellite's lifetime. The intervals where the SAO estimates show significant deviations from the nominal values are given in the appendix. In the currently active constellation 10 satellites are affected.

Figure 5 summarizes the re-estimated SAO values. Many of the corrections have a magnitude of 10 to 15 cm – however also smaller corrections can be found. No dominant direction may be identified for these re-estimated SAO values. It is remarkable that in few cases the SAO corrections reassume the nominal value (e.g., satellites with SVN 721 or SVN 744).

Since in none of the cases a significant change in the Z-component of the SAO was detected, only the horizontal corrections were extracted from the long-term estimation and used in the validation procedures presented in Sect. 4 . For all remaining intervals, as well as for the Z-components of the antenna corrections, the original values of the IGS 08 antenna model were used. Also the satellite antenna phase center pattern have been reused from the IGS 08 antenna model because a re-estimation in the detected intervals did not show any significant deviations.

4. Validation

The same NEQs and processing strategy as described in Sect. 2 were also used for the validation. The re-estimated SAO values according to Table A.2 are introduced instead of the nominal values from the IGS 08 antenna model (Schmid et al, 2016). The orbits used for the validation procedure are in general the extracted middle day of the three-day long-arc solution (with some exceptions discussed in Sect. 4.3). For the datum definition only no-net-rotation and no-net-translation conditions with respect to ITRF2014 for the verified reference frame sites (same as in Sect. 3.1) are applied according to the usual practice within the IGS .
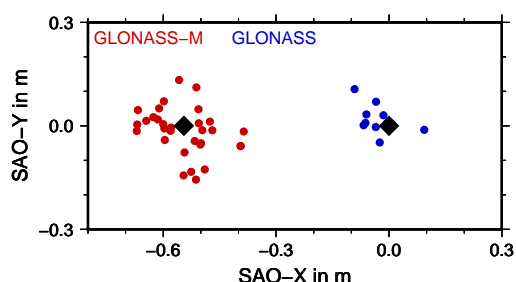

Figure 5: Estimated SAO values (filled circles) compared to the nominal values (black diamonds).

4.1. Estimated solar radiation pressure parameters

In the orbit determination procedure the GNSS observations refer to the satellite antenna phase center. The SAO corrections together with satellite antenna phase center variations are used to obtain the instantaneous location of the satellite's center of mass to which the equation of motion and related parameters are referring. If wrong SAO corrections are applied, the series of satellite positions that have to be represented by the equation of motion will differ from the real satellite trajectory in a systematic way (depending on the orientation of the satellite). This difference may partly be absorbed by the estimated orbit parameters (mainly SRP parameters).

As an example Fig. 6 shows the estimated SRP parameters for two GLONASS satellites. The identified discontinuities in the SAO parameters are indicated by vertical lines. The first letter of the label in the plots denotes the component of the Sun-oriented coordinate system at the satellite (as it has been used in Arnold et al, 2015), where D points towards the Sun, Y along the axis of the solar panels and B completes the right-handed system. The number 0 indicates the constant term of the component, whereas 1 is related to once-per-revolution and 2 to twice-per-revolution periodic terms. For the periodic terms the third letter C or S denotes the cosine and sine components, respectively.

The solar panels are pointing towards the Sun due to the attitude control of the GLONASS satellites (apart form short periods during the noon-turn operation). So, the direct SRP effect is causing a constant force in the $D0$ component. At the same time, also a part of the satellite body is contributing to this parameter. Depending on the geometry between Earth, satellite and Sun, different parts of the satellite body contribute to the $D0$ term as well. In particular with the elongated body of the GLONASS satellites a pattern in the estimated SRP parameters is expected. This consideration implies that the pattern should continue also after the detected events in the SAO correction time series.

The green dots in Fig. 6 are the SRP parameters from the solution with the nominal SAO corrections from the IGS 08 antenna model. In particular the characteristics of the $D0$- and the $B0$-components change notably after the first discontinuity in the SAO estimates. The corresponding cosine terms are also affected. The SRP parameters obtained from the orbit determination using the re-estimated SAO values are plotted in red dots. Here the changes in the pattern are much less pronounced after the epochs of the SAO discontinuities. This may indicate that the estimated SRP parameters need to absorb less artifacts between the trajectory indicated by the GNSS measurements and the equation of motion. Whether the orbits have a better quality will be assessed in the subsequent sections.

6

(a) Satellite SVN 736, slot number R09 and R16

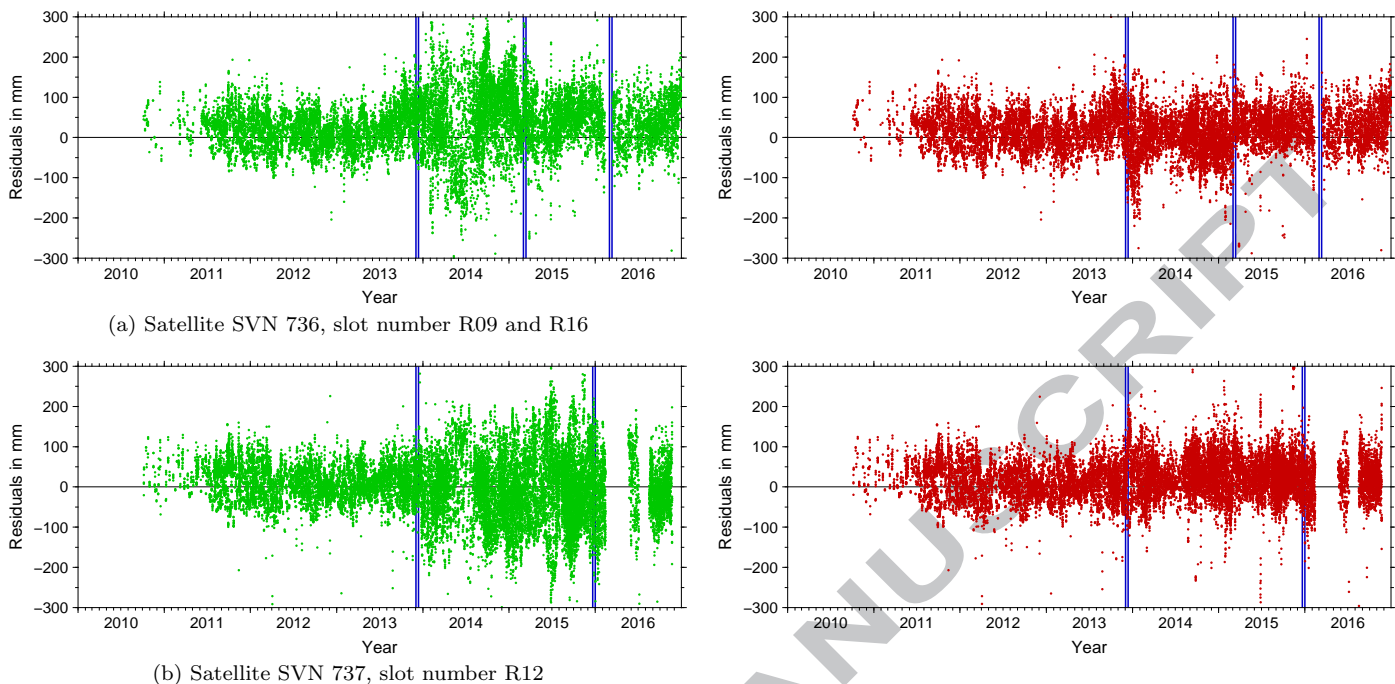(b) Satellite SVN 737, slot number R12

Figure 7: SLR residuals with the original (left panels) and the re-estimated (right panels) SAO corrections. The vertical blue lines indicate the epochs where the used SAO values do change.

4.2. SLR residuals

SLR is a well-established independent technique to verify orbits of GNSS satellites. A common way is to take the satellite positions from a microwave-derived orbit solution and the SLR station coordinates from a reference frame solution, which is expected to be consistent with the one that has been used to generate the orbit solution. If in both cases the ITRF2014 coordinates are used, this consistency can be assumed. The geometric distance is directly compared to the SLR measurements after applying the standard corrections (e.g., for the troposphere delay). These observed-minus-computed values are typically named SLR residuals. A detailed discussion of particular issues, e.g., related to single-photon or multi-photon SLR receiving stations, with this approach is for instance given in Sośnica et al (2015).

Although all GLONASS satellites are equipped with SLR reflectors, the International Laser Ranging Service (ILRS, Pearlman et al, 2002) decided to track only three and later six of them (one or two in each plane). Meanwhile some of the SLR tracking stations developed the capacity to extend the tracking to the full GLONASS constellation (SLR tracking station Herstmonceux started in 2010, see Appleby et al, 2012, other stations followed shortly later). Since 2011 a reasonable amount of SLR tracking data to nearly all active GLONASS satellites is available.

Typical examples of the time series of SLR residuals for two satellites (the same two satellites as shown in Fig. 6) are shown in Fig. 7. A clear improvement is visible between the left panel (using the original SAOs) and the right

one (using the re-estimated SAOs). The vertical lines indicate the intervals where used SAO corrections are changing on the right hand panels. Even if there are intervals where the SLR residuals are still slightly elevated (e.g., second interval for satellite SVN 736 in Fig. 7a) there is significant improvement by reducing the scatter. The better homogeneity of the patterns in the estimated SRP parameters is confirmed as an orbit improvement.

Figure 8 gives an overview of the statistics of the SLR residuals. The green bars refer to the orbit solution using the original SAO values, whereas the red bars refer to the orbits using the re-estimated ones. The bars cover the range from the 25% to the 75% quantile value, implying that the length of the bar represents the interquartile range (IQR). The dot indicates the median (50% quantile) of all SLR residuals to a particular satellite obtained over one year. It is clearly visible that the scatter of the SLR residuals (length of the bars) is reduced and becomes more consistent in time using the re-estimated SAOs. The magnitude of the difference between the original and re-estimated SAO corrections in the X- and Y-component ($dSAO = \sqrt{\Delta X^2 + \Delta Y^2}$, please find the exact values in Tab. A.2) is given on the top of each panel for the individual satellites. A darker gray (black for 15 cm or more) is related to a bigger deviation.

This confirms the improvement of the GLONASS orbits, in particular in the radial direction. In some cases (e.g., satellites 723, 725, or 732) the scatter of the SLR residuals is reduced by up to a factor of two. In other cases (e.g., satellite 730 or 736), the improvement is related to the long-term stability of the median (and quantile values).
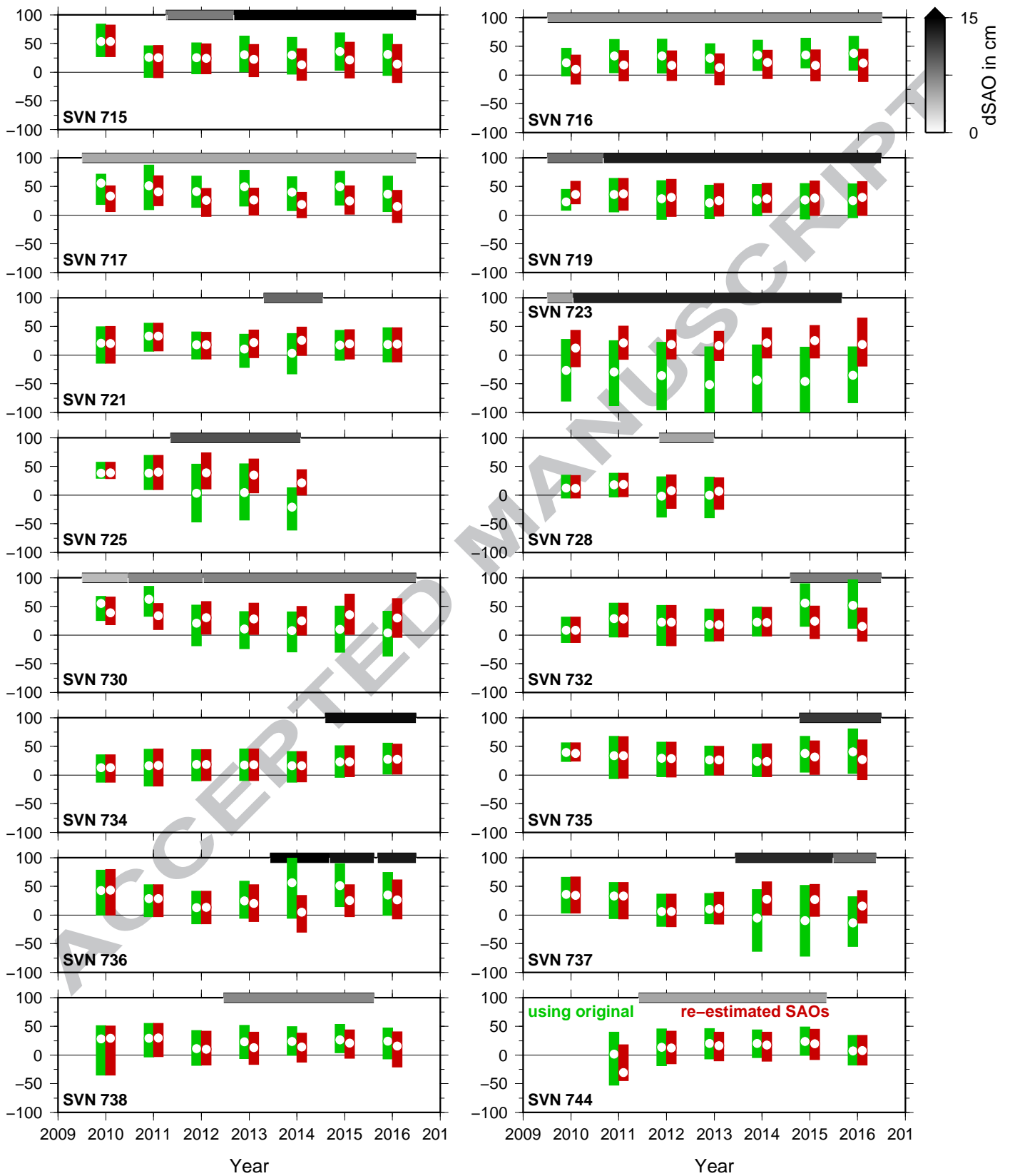
Figure 8: Statistics on the SLR residuals to a certain satellite obtained within a year. The green and red bars cover the range from the quantile 25% to 75%. The white dot indicates the corresponding median value. All SLR residuals are given in mm. The gray line on top of the plots indicate the magnitude of the difference between the original and re-estimated SAO corrections during a given interval.

8
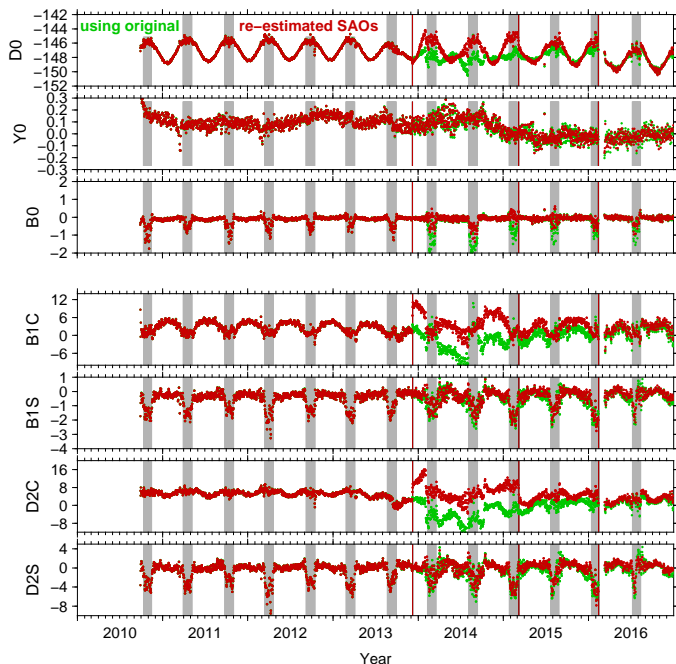
(a) Satellite SVN 736, slot number R09 and R16
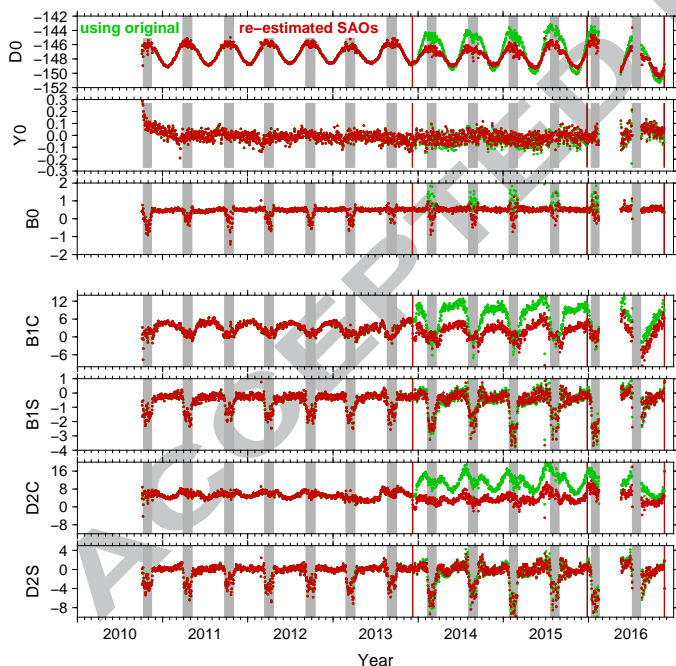
(b) Satellite SVN 737, slot number R12

Figure 6: Estimated SRP parameters using the original (green dots) and re-estimated (red dots) SAO corrections. The vertical lines indicate the epochs of detected discontinuities in the SAO time series, whereas the gray shaded areas are allocated to the eclipse seasons. See text for the description of the parameter names. All values are given in nm/s^2 .

For satellite 744 and the year 2011 the red bars seem to indicate a degradation of the orbit quality (median value at -4 cm whereas the other years show median values of $+1\ldots 2$ cm). This can be explained by the low number of SLR measurements to this particular satellite obtained in the year 2011 (68 normal points compared to $1\,500\ldots 5\,000$ as typically available for the statistics per satellite and year – depending on the priority of the particular satellite in the SLR tracking network).

4.3. Orbit misclosures

Another way to evaluate the quality of the GLONASS orbits is to check the consistency of consecutive orbit arcs – the so called orbit misclosures: the discontinuities at the end of the daily orbit arcs are computed. The end of the orbital arc is the weakest part due to the related error propagation. Due to the sparse network density in the early years (before 2006) the orbit misclosures for the GLONASS satellites from one-day arcs have a magnitude of about 20 cm or even above. This number reduces to 6 to 7 cm for the years after 2010 – total difference over all components with (as usual) the biggest contribution from the along-track and the smallest from the out-of-plane component.

For that reason, CODE is typically producing orbits based on longer arcs, e.g., over three days. The orbit misclosures at the ends of the long arcs (e.g., arc over days $n\ldots n+2$ with the arc over the days $n+3\ldots n+5$ at the common midnight epoch at day $n+2$ at 24:00:00) are – as in Section 6 of Lutz et al (2016) – still in the same order of magnitude as those for the one-day arcs. This confirms that the orbit model can represent the satellite motion also over 72 hours without any limitations. The picture changes when extracting the middle day as the solution for the orbit determination. In the early years (before 2006) the magnitude of the orbit misclosures between consecutive middle day extractions is typically in the order of 5 cm. After 2010, when a global coverage with GLONASS tracking stations is achieved, the orbit misclosures become about 1.5 cm .

The detected events in the re-estimated SAO correction time series have different impacts on the orbit misclosures. This is illustrated in Tab. 1 where gray-shaded cells indicate years where a re-estimated SAO value was used. The biggest increase of the orbit misclosures was detected for the SVNs 735 and 736 with a factor of two. In other cases (e.g., SVN 734, 737, 738) the magnitude of the misclosures increases as well, but to a lower extent. Interestingly there are also examples (e.g., SVN 732 but also 701, 783, 788, not in the table) where no significant change in the orbit misclosures have been detected.

Using the re-estimated SAO corrections instead of the nominal ones, a part of the increased orbit misclosures was compensated. The biggest positive effect of about 10% was observed in the out of plane component. In the along-track component an improvement of up to 5% was achieved whereas in the radial component nearly no effect

9

Table 1: Orbit misclosures (total over all components) for a subset of GLONASS satellites using the original or re-estimated SAO corrections (1-sigma). The gray shaded cells are years where for a particular satellite re-estimated SAO corrections are available. All values are given in mm.

Sat.	SAO	2010	2011	2012	2013	2014	2015	2016
730	orig.	87	83	96	88	86	103	100
	re-est.	88	85	100	90	85	99	103
732	orig.	75	60	59	66	52	57	56
	re-est.	74	60	61	64	51	55	57
734	orig.	66	72	70	55	57	114	116
	re-est.	66	72	69	55	57	106	112
735	orig.	90	93	89	87	77	111	120
	re-est.	88	93	84	89	75	100	118
736	orig.	51	78	65	66	114	100	104
	re-est.	53	76	63	63	117	87	91
737	orig.	65	67	65	66	114	108	164
	re-est.	67	67	65	65	112	108	164
738	orig.	87	69	64	83	85	69	90
	re-est.	89	67	63	78	78	60	98
744	orig.		61	70	79	70	58	45
	re-est.		52	67	71	68	59	45

was detected. Consequently the improvement in the total over all three components that is shown in Tab. 1 in most cases below 5% – meaning far away to being significant. There are also examples for degradation within the noise level of the orbit misclosures based on one-day arcs. The use of the re-estimated SAO corrections cannot fully compensate the effect in the satellite orbit modelling to the full extent in terms of orbit misclosures for one-day arcs. Whether and to which extent this is related to the dependency from the geometry of the tracking stations (reported by Ortiz Geist et al, 2016) is not clear to far.

5. Discussion

The shift of the nominal satellite antenna phase center vector, as suggested by the re-estimated SAO corrections (see Sect. 3.3), can be explained in different ways. Which of the potential reasons really applies cannot be definitively concluded without having further details from the system provider. Nevertheless potential explanations shall be discussed. To support the discussion Fig. 9 contains a picture of a GLONASS-M satellite with some basic dimensions.

1. Assuming a total mass of the satellite of about 1.5 t and a radius of the cylinder with about 0.5 m a shift of the center of mass of the satellite by 10 cm is rather unrealistic.

2. A 10 cm bias in SAO estimates can, for instance, be explained by misalignement of the satellite towards the Earth by $\frac{10\,\text{cm}}{1.87\,\text{m}} \Rightarrow 3°$. In the Z-component this
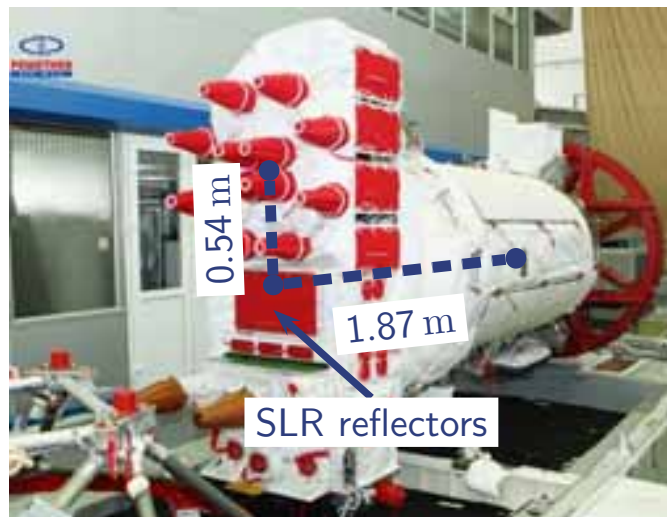

Figure 9: Picture of a GLONASS-M satellite with selected dimensions. From http://spaceflight101.com/spacecraft/glonass-m/.

results in a difference of 2 mm which is a magnitude that is too small to be detectable in the GNSS observations. A misalignment of the satellite attitude of only 3° still allows to track the signal of the satellite.

3. The L-band antenna of GLONASS satellites consists of four segments (may also be seen in Fig. 9). If one of the segments fails, a change in the effective horizontal SAO is expected. Even if the emission power of the GNSS signal is reduced, the GNSS tracking stations may still receive the signal.

5.1. Statistics on SLR residuals

If the change of the SAO corrections is caused by the electronics related to the L-band antennas only the microwave data are affected. If there is an issue with the attitude control also the SLR measurements are affected. Since the amount of available SLR measurements is too small, a direct estimation of the position of the retroreflector with respect to the center of mass (CoM) is not possible with sufficient accuracy.

Nevertheless, the GLONASS orbits based on the re-estimated SAO values may be confronted with the SLR measurements twice: once using the original vector from the satellite CoM to the location of the SLR reflector (as given by the ILRS) and a second time where the vector is modified by the same corrections as applied to the microwave antenna based on the estimation described in Sect. 3. In such an analysis, the IQR of the SLR residuals is in the order of 5 cm for satellites where at least 10 000 measurements are available between 2010 and end of 2016.

However, comparing both series of SLR residuals with the different assumptions on the vector from the CoM to the retroreflector shows only small differences ($< 5\%$), which unfortunately does not allow to answer the question about the source of the observed effect. Another fact

10

should be also considered when interpreting the SLR residual statistics in this context: first the microwave antenna at the GLONASS-M satellites is located at $X = -0.545\,\mathrm{m}$ in the satellite body-fixed coordinate system. The SLR reflector has only an eccentricity of $X = 0.137\,\mathrm{m}$. The effect observed at the microwave antenna is reduced by a factor of about four at the SLR antenna if the satellite is tilted. Secondly, SLR observations are range measurements and, therefore, only the projection of a potential eccentricity with respect to the direction to the tracking station is visible in the residuals.

5.2. Assessment of code bias

The SAO corrections obtained in Sect. 3.3 are only based on carrier phase observations. From a recently generated reprocessing series related for ionosphere products a consistent set of code biases is available at AIUB since 2010. Code biases are typically represented as Differential Code bias (DCB) or according to Villiger et al (2017) also as observable-specific signal biases (OSB) for – among others – GLONASS satellites. Independent from the representation a time series analysis regarding discontinuities are possible that may indicate changes in the hardware delay at the satellite.

Only three events in the time series of code biases do coincide with the epoch of events in the SAO parameters. In February 2015, there was a simultaneous discontinuity in the DCB as well as in the SAO series for satellite SVN 732 ($\Delta SAO \approx 8\,\mathrm{cm}$ versus $\Delta DCB(P2-C2) = +3\,\mathrm{ns}$ and $\Delta DCB(P1-P2) = -3\,\mathrm{ns}$). There is only one event for SVN 730 in June 2012 with a comparable magnitude of discontinuities.

One more event for SVN 701 in April 2008 was found where only the $DCB(P1-P2)$ show a discontinuity at the same epoch as the event in the SAO with a magnitude of 5 ns whereas the other DCBs are continuous. This means that the hardware delays for the signals in the first and second frequencies are differently effected but those on the same frequency are consistently affected. In all other cases where discontinuities in the SAO correction series have been detected, the DCB time series do not show any significant event (i.e., $\geq 1\,\mathrm{ns}$) at the same epochs.

In conclusion it is likely that the events related to satellite hardware delays for the pseudorange measurements are independent from the events in the SAO corrections investigated in the previous sections.

6. Summary and Conclusions

For a number of GLONASS satellites a significant increase of the SLR residuals was observed based on the most recent reprocessing campaign carried out at AIUB in the frame of the EGSIEM project. This observation is confirmed by using orbits from other IGS analysis centers that provide GLONASS orbits. It was also noticed that many of the affected satellites have reduced dual-frequency

tracking (only measurements on one of the two frequencies are reported in the Receiver INdependent EXchange format (RINEX) observation files). Even if this amount is up to 10 times of the usual amount (e.g., due to weak signal in low elevations), an orbit determination is still possible for these satellites.

The satellite antenna offset corrections for the satellites were re-estimated and deviations from the manufacturer values, that are typically used by the IGS analysis centers, of up to 15 cm in the horizontal components were detected. There are also numerous cases where the time series of estimated SAO corrections show discontinuities. Applying the re-estimated SAO corrections in the parameter estimation process, the orbit verification by SLR measurements shows a reduction to the same level as for all other satellites.

It cannot be definitely concluded what is causing the observed deviation of the horizontal SAO corrections with respect to the nominal values. There is at least no strong relation of detectable events with discontinuities in the time series of the satellite code biases. A reduced carrier-to-noise density reported in the observation RINEX files from different, globally distributed stations at least for some of the events suggests an issue with the satellite antenna or the related electronics. For a more detailed diagnostics more information from the system provider would be necessary.

The intervals for which re-estimated SAO corrections were determined and used in the validation procedure in the frame of this study are listed in the appendix. It is recommended to utilize these values for processing of GLONASS data in future. According to the usual verification procedure in the IGS a second, independent solution is appreciated in order to compare and potentially combine these results.

Acknowledgements

Appendix A. Appendix: List of Events

Table A.2 provides a list of events detected in the frame of this study during the interval between 2002 until March 2016 (see explanation in Sect. 3.2). The intervals where the re-estimated SAOs corrections have been applied are indicated.

Altamimi Z, Rebischung P, Métivier L, Collilieux X (2016) ITRF2014: A new release of the International Terrestrial Reference Frame modeling nonlinear station motions. Journal of Geophysical Research 121(8):6109–6131, DOI 10.1002/2016JB013098

Appleby G, Gibbs P, Potter C, Sherwood R, Shoobridge T, Smith V, Wilkinson M (2012) ILRS Station Reports: Herstmonceux, UK. In: Noll C, Pearlman M (eds) International Laser Ranging Service (ILRS) 2009-2010 Report, Goddard Space Flight Center, Greenbelt, MD, pp 12–34–12–38

Arnold D, Meindl M, Beutler G, Dach R, Schaer S, Lutz S, Prange L, Sośnica K, Mervart L, Jäggi A (2015) CODE's new solar radiation pressure model for GNSS orbit determination. Journal of Geodesy 89(8):775–791, DOI 10.1007/s00190-015-0814-4

Beutler G, Brockmann E, Gurtner W, Hugentobler U, Mervart L, Rothacher M, Verdun A (1994) Extended orbit modeling techniques at the CODE processing center of the International GPS Service for Geodynamics (IGS): Theory and initial results. Manuscripta Geodaetica 19(6):367–386

Beutler G, Brockmann E, Hugentobler U, Mervart L, Rothacher M, Weber R (1996) Combining consecutive short arcs into long arcs for precise and efficient GPS orbit determination. Journal of Geodesy 70(5):287–299, DOI 10.1007/BF00867349

Böhm J, Werl B, Schuh H (2006) Troposphere mapping functions for GPS and VLBI from ECMWF operationals analysis data. Journal of Geophysical Research 111(B2):B02,406, DOI 10.1029/2005JB003629

Bruyninx C, Araszkiewicz A, Brockmann E, Kenyeres A, Legrand J, Liwosz T, Mitterschiffthaler P, Pacione R, Söhne W, Völksen C (2018) EUREF permanent network: IGS Technical Report 2017. In: Villiger A, Dach R (eds) International GNSS Service: Technical Report 2017, IGS Central Bureau, pp 105 – 116

Chen G, Herring TA (1997) Effects of atmospheric azimuthal asymmetry on the analysis of space geodetic data. Journal of Geophysical Research 102(B9):20,489–20,502, DOI 10.1029/97JB01739

Dach R, Brockmann E, Schaer S, Beutler G, Meindl M, Prange L, Bock H, Jäggi A, Ostini L (2009) GNSS processing at CODE: Status report. Journal of Geodesy 83(3–4):353–365, DOI 10.1007/s00190-008-0281-2

Dach R, Lutz S, Walser P, Fridez P (eds) (2015) Bernese GNSS Software, Version 5.2. Astronomical Institute, University of Bern, Bern, Switzerland, DOI 10.7892/boris.72297, URL ftp://ftp.aiub.unibe.ch/BERN52/DOCU/DOCU52.pdf, user manual

Dilssner F, Dach R, Schmid R, Springer TA, Zandbergen R (2011) Updating the IGS processing standard: new GLONASS satellite antenna corrections for igs08.atx. In: EGU General Assembly, Vienna, Austria, poster

Grahsl A, Sušnik A, Prange L, Arnold D, Dach R, Jäggi A (2016) GNSS orbit validation activities at the Astronomical Institute in Bern. In: Proceedings of the 20th International Workshop on Laser Ranging, October 10–14, 2016, Potsdam, Germany

Jäggi A, Jean Y, Meyer U, Sušnik A, Weigelt M, van Dam T, Li Z, Flechtner F, Gruber C, Güntner A, Gouweleeuw B, Mayer-Gürr T, Kvas A, Martinis S, Zwenzer H, Bruinsma S, Lemoine JM, Flury J, Bourgogne S, Steffen H, Horwath M (2015) European Gravity Service for Improved Emergency Management - project overview and first results. In: AGU fall meeting, AGU, San Francisco, presentation

Johnston G, Riddell A, Hausler G (2017) The International GNSS Service. In: Teunissen P, Montenbruck O (eds) Springer Handbook of Global Navigation Satellite Systems, Cham, Switzerland: Springer International Publishing, pp 967–982, DOI 10.1007/978-3-319-42928-1

Kouba J (2009) A simplified yaw-attitude model for eclipsing GPS satellites. GPS Solutions 13(1):1–12, DOI 10.1007/s10291-008-0092-1

Lutz S, Meindl M, Steigenberger P, Beutler G, Sośnica K, Schaer S, Dach R, Arnold D, Thaller D, Jäggi A (2016) Impact of the arc length on GNSS analysis results. Journal of Geodesy 90(4):365–378, DOI 10.1007/s00190-015-0878-1

Montenbruck O, Steigenberger P, Prange L, Deng Z, Zhao Q, Perosanz F, Romero I, Noll C, Stürze A, Weber G, Schmid R, MacLeod K, Schaer S (2017) The Multi-GNSS Experiment (MGEX) of the International GNSS Service (IGS) – Achievements, prospects and challenges. Advances in Space Research 59(7):1671–1697, DOI 10.1016/j.asr.2017.01.011, article

Moore M, Herring T (2018) Analysis center coordinator: IGS Technical Report 2017. In: Villiger A, Dach R (eds) International GNSS Service: Technical Report 2017, IGS Central Bureau, pp 23 – 31

Ortiz Geist E, Dach R, Schönemann E, Enderle W, Jäggi A (2016) Influence of station distribution on GNSS satellite orbits. In: IGS Workshop, Sydney, Australia.

Pearlman MR, Degnan JJ, Bosworth JM (2002) The International Laser Ranging Service. Advances in Space Research 30(2):135–143, DOI 10.1016/S0273-1177(02)00277-6

Prange L, Orliac E, Dach R, Arnold D, Beutler G, Schaer S, Jäggi A (2016) CODE's five-system orbit and clock solution—the challenges of multi-GNSS data analysis. Journal of Geodesy 91(4):345–360, DOI 10.1007/s00190-016-0968-8

Schmid R, Rothacher M (2003) Estimation of elevation-dependent satellite antenna phase center variations of GPS satellites. Journal of Geodesy 77(7–8):440–446, DOI 10.1007/s00190-003-0339-0

Schmid R, Steigenberger P, Gendt G, Ge M, Rothacher M (2007) Generation of a consistent absolute phase center correction model for GPS receiver and satellite antennas. Journal of Geodesy 81(12):781–798, DOI 10.1007/s00190-007-0148-y

Schmid R, Dach R, Collilieux X, Jäggi A, Schmitz M, Dilssner F (2016) Absolute IGS antenna phase center model igs08.atx: status and potential improvements. Journal of Geodesy 90(4):343–364, DOI 10.1007/s00190-015-0876-3

Sośnica K, Thaller D, Dach R, Steigenberger P, Beutler G, Arnold D, Jäggi A (2015) Satellite Laser Ranging to GPS and GLONASS. Journal of Geodesy 89(7):725–743, DOI 10.1007/s00190-015-0810-8

Springer TA (1999) Modeling and Validating Orbits and Clocks Using the Global Positioning System. PhD thesis, Astronomical Institute, University of Berne, Bern, Switzerland

Springer TA, Dach R (2010) GPS, GLONASS, and more. GPS World 21(6):48–58, URL http://www.nxtbook.com/nxtbooks/questex/gps0610/index.php#/44

Steigenberger P, Lutz S, Dach R, Schaer S, Jäggi A (2014) CODE repro2 product series for the IGS. DOI 10.7892/boris.75680, URL http://www.aiub.unibe.ch/download/REPRO_2013

Sušnik A, Grahsl A, Arnold D, Villiger A, Dach R, Jäggi A (2017) GNSS reprocessing results in the framework of the EGSIEM project. Journal of Geodesy In review

Villiger A, Schaer S, Dach R, Prange L, Jäggi A (2017) Determination of multi-GNSS pseudo-absolute code biases and verification of receiver tracking technology. In: EGU General Assembly, Vienna, Austria

Willis P, Slater J, Beutler G, Gurtner W, Noll C, Weber R, Neilan RE, Hein G (2000) The IGEX-98 campaign: Highlights and perspective. In: Schwarz KP (ed) Geodesy Beyond 2000, The Challenges of the First Decade, Springer Berlin Heidelberg, International Association of Geodesy Symposia, vol 121, pp 22–25, DOI 10.1007/978-3-642-59742-8_4

Table A.2: Listing of all intervals with re-estimated SAO corrections derived for GLONASS satellites in the frame of this study during the interval between 2002 until March 2016 (see explanation in Sect. 3.2).

Satellite		Affected interval		ΔX	ΔY	SAO-X	SAO-Y	
SVN	PRN	start date	end date	in meters	in meters	in meters	in meters	Satellite type
701	R06	2008 04 27	2009 09 13	-0.1240	0.0037	-0.6691	0.0037	GLONASS-M
713	R24	2005 12 25	2010 02 28	-0.0507	-0.0412	-0.5957	-0.0412	GLONASS-M
714	R23	2006 02 28	2010 03 18	0.1507	-0.0586	-0.3943	-0.0586	GLONASS-M
714	R06	2010 04 28	2010 09 30	0.1507	-0.0586	-0.3943	-0.0586	GLONASS-M
714	R17	2010 12 16	2011 12 19	0.1507	-0.0586	-0.3943	-0.0586	GLONASS-M
714	R18	2014 02 16	2014 04 10	0.1507	-0.0586	-0.3943	-0.0586	GLONASS-M
714	R17	2015 04 13	2016 02 23	0.1507	-0.0586	-0.3943	-0.0586	GLONASS-M
715	R14	2011 10 02	2013 03 06	0.0016	-0.0772	-0.5434	-0.0772	GLONASS-M
715	R14	2013 03 07		0.0319	-0.1560	-0.5131	-0.1560	GLONASS-M
716	R15	2006 12 25		0.0387	0.0479	-0.5063	0.0479	GLONASS-M
717	R10	2006 12 25		0.0488	-0.0127	-0.4962	-0.0127	GLONASS-M
718	R17	2007 10 26	2010 12 15	0.0454	-0.0505	-0.4996	-0.0505	GLONASS-M
719	R20	2007 10 26	2011 03 05	-0.0660	0.0504	-0.6110	0.0504	GLONASS-M
719	R20	2011 03 06		-0.0128	0.1329	-0.5578	0.1329	GLONASS-M
721	R13	2013 10 20	2015 01 17	-0.0533	0.0712	-0.5983	0.0712	GLONASS-M
722	R09	2007 12 25	2010 09 30	-0.0354	-0.0144	-0.5804	-0.0144	GLONASS-M
723	R11	2007 12 25	2010 07 17	-0.0550	0.0049	-0.6000	0.0049	GLONASS-M
723	R11	2010 07 18	2016 03 02	-0.1222	0.0457	-0.6672	0.0457	GLONASS-M
725	R21	2011 11 06	2014 07 31	-0.1002	0.0144	-0.6452	0.0144	GLONASS-M
726	R22	2008 09 25	2010 02 28	-0.0343	-0.0050	-0.5793	-0.0050	GLONASS-M
728	R02	2012 05 06	2013 06 29	-0.0523	-0.0077	-0.5973	-0.0077	GLONASS-M
730	R01	2009 12 14	2010 12 18	0.0396	0.0073	-0.5054	0.0073	GLONASS-M
730	R01	2010 12 19	2012 07 14	0.0688	0.0121	-0.4762	0.0121	GLONASS-M
730	R01	2012 07 15		-0.0694	0.0184	-0.6144	0.0184	GLONASS-M
732	R23	2015 02 01		0.0753	-0.0130	-0.4697	-0.0131	GLONASS-M
734	R05	2015 02 01		-0.0009	-0.1437	-0.5459	-0.1437	GLONASS-M
735	R24	2015 04 12		0.0329	0.1116	-0.5121	0.1116	GLONASS-M
736	R09	2013 12 08	2015 03 07	0.1589	-0.0166	-0.3861	-0.0166	GLONASS-M
736	R09	2015 03 08	2016 02 12	0.0554	-0.1265	-0.4896	-0.1265	GLONASS-M
736	R16	2016 03 07		0.0192	-0.1335	-0.5258	-0.1335	GLONASS-M
737	R12	2013 12 08	2015 12 26	-0.1254	-0.0149	-0.6704	-0.0149	GLONASS-M
737	R12	2015 12 27	2016 11 20	-0.0814	0.0252	-0.6264	0.0252	GLONASS-M
738	R16	2012 12 16	2016 02 13	0.0434	-0.0545	-0.5016	-0.0545	GLONASS-M
744	R03	2011 12 01	2015 11 07	0.0285	-0.0440	-0.5165	-0.0440	GLONASS-M
779	R01	1999 01 01	2002 07 08	0.0936	-0.0116	0.0936	-0.0116	GLONASS
783	R18	2000 10 13	2004 06 26	-0.0600	0.0330	-0.0600	0.0330	GLONASS
783	R18	2004 06 27	2007 05 24	-0.0914	0.1064	-0.0914	0.1064	GLONASS
788	R24	2003 09 07	2005 12 24	-0.0345	0.0698	-0.0345	0.0698	GLONASS
789	R03	2001 12 01	2008 12 24	-0.0149	0.0308	-0.0149	0.0308	GLONASS
791	R22	2002 12 25	2007 10 25	-0.0247	-0.0482	-0.0247	-0.0482	GLONASS
792	R21	2006 05 21	2008 09 24	-0.0626	0.0083	-0.0626	0.0083	GLONASS
796	R01	2004 12 26	2009 12 13	-0.0352	-0.0035	-0.0352	-0.0035	GLONASS
798	R19	2005 12 25	2007 10 25	-0.0675	0.0018	-0.0675	0.0018	GLONASS